Crack path and liquid metal embrittlement specificity of austenitic steels in mercury at room temperature

Thierry Auger, PhD [a,b,*], Bassem Barkia, PhD [b], Eva Héripré, PhD [b], Vincent Michel, M. Sc. [a], Denis Mutel, M. Sc. [b], Ivan Guillot, PhD [c], Zehoua Hamouche, PhD [a], Liliana Medina-Almazàn, PhD [b,d]

[a] PIMM/Arts et Métiers Institute of Technology, CNRS, Cnam, HESAM University, 151 boulevard de l'hôpital, Paris 75013, France
[b] Université Paris-Saclay, CentraleSupélec, CNRS, Laboratoire de Mécanique des Sols, Structures et Matériaux, Gif-sur-Yvette 91190, France
[c] ICMPE/CNRS, UPEC, 2 Rue Henri Dunant, Thiais 94320, France
[d] CFE, Carretera Cardel- Nautla Km 42.5, Alto Lucero, Veracruz 91476, Mexico

A B S T R A C T

A liquid metal embrittlement specificity of three austenitic steels with increasing nickel content (304 L, 316 L and 316L(N)) is studied in liquid mercury in the axisymmetric notched geometry. Only the low nickel alloys are susceptible to LME. The crack path of an austenitic steel fracture induced by liquid mercury has been elucidated at microstructural scale. Deformation induced martensite (γ(fcc) → α'(bcc)) of the low nickel steels induces numerous α'/α' interfaces at small scale that are susceptible to be embrittled. Because the only steel that resists LME is the one that shows stability over α' phase change due mostly to its higher nickel content, a point confirmed by X Ray fractography, it is inferred that the major factor contributing to the LME sensitivity at room temperature is the α' phase formation in unstable austenitic steels during plastic strain. This provides a sound rationale on how to prevent mercury induced embrittlement with austenitic steels.

Introduction

Austenitic stainless steels are the structural materials of choice for containment of liquid metals in many applications. Understanding their mutual chemical or physical interactions such as corrosion or liquid metal embrittlement (LME) is therefore highly desirable. While austenitic steels have been rather thoroughly investigated for liquid metal corrosion (in PbBi for example [1]), the LME phenomenology of austenitic steels is still not satisfactorily understood. A screening study in mercury by Krupowitz with several austenitic stainless steels indicates that the 304, 304 L and 321 steels are susceptible to LME in mercury at room temperature but not the 316 and 316 L steels [2]. The study was focused on uniaxial mechanical testing and the fractographic study that was carried out gave no particular rationale for the observed variation in LME sensitivity. In a work on oligocyclic fatigue of 316LN at room temperature, a mild reduction in the lifetime of the samples was observed when exposed to liquid mercury [3]. Another study showed significant LME in plane stress fracture mechanics experiments with 316 L in contact with mercury [4]. This spread in the sensitivity with 316 L steels seems to obfuscate the issue of LME in this environment with contradicting statements. A matter, maybe not given sufficient consideration, is the unstable behavior of some of the austenitic steels when plastically strained leading to a γ(fcc) to α'(bcc) phase transformation [5]. One can indeed notice when considering the steel's composition, that those showing LME sensitivity are low nickel austenitic steels (see compositions given in [2–4]). Therefore, one may infer that the LME sensitivity could be connected to or triggered by the Deformation Induced Martensite (DIM) transformation, a behavior mainly controlled by the nickel content when varying composition [6]. This possibility was already hinted by the behavior of the 304 L steel in sodium where detailed small-scale analysis showed that γ/α' and α'/α' interfaces are the fracture crack path [7,8]. A strong correlation of the LME trend with the amount of DIM was also recently unveiled on a low nickel version of the 316 L steel in contact with eutectic gallium-indium melt [9]. The LME sensitivity of austenitic steels with Hg would therefore have to be attributed essentially to a LME sensitivity of the bcc phase formed during plastic deformation.

The work described in this paper allows to settle this question in mercury by specifically varying the amount of nickel around the critical concentration for a drastic change in the DIM at room temperature. An

* Corresponding author at: PIMM/Arts et Métiers Institute of Technology, CNRS, Cnam, HESAM University, 151 boulevard de l'hôpital, Paris 75013, France.
E-mail addresses: thierry.auger@ensam.eu (T. Auger), Bassem.BARKIA@ensam.eu (B. Barkia), eva.heripre@centralesupelec.fr (E. Héripré), vincent.michel@ensam.eu (V. Michel), denis.mutel.1@ulaval.ca (D. Mutel), ivan.guillot@cnrs.fr (I. Guillot), zehoua.hamouche@ensam.eu (Z. Hamouche), liliana.medina@cfe.gob.mx (L. Medina-Almazàn).

https://doi.org/10.1016/j.scriptamat.2022.114733

Table 1.
304 L, 316 L and 316L(N) elemental composition from suppliers (* not measured). Note that the equivalent nickel content is given in parenthesis (Pryce and Andrew formulae [11]).

Élément in%wt	Cr	Ni in%wt (%Eq.)	Mo	Mn	C*	Si	P	S	Cu	Co	N	Ti	Al
304L	18.6	9.0 (10.0)	N/A*	1.48	0.015	0.42	0.023	0.001	*	0.1	*	*	*
316L	16.8	10.2 (11.72)	2.1	1.8	0.016	0.64	0.026	0.03	0.23	*	0.025	0.006	0.018
316L(N)	17.9	12.1 (14)	2.35	1.72	0.012	0.45	0.034	0.025	0.00025	0.0008	0.07	0.0015	0.0025

experimental investigation at small-scale is first carried out to characterize further mercury induced microstructural crack path. We then chose to test and analyze the LME behavior of 304 L (9wt% Ni), a low nickel version of 316 L (10wt% Ni) and a nuclear grade of nitrogen stabilized 316 L, the 316L(N) (with 12 wt% Ni). Increasing the nickel content with these three materials procures a higher stability relative to DIM. Nitrogen has also the ability to stabilize austenite relative to the phase diagram but does not contribute to suppress DIM [6]. The fraction of γ to α' phase transform upon fracture was assessed by XRay fractography, a technique used up to now mainly for characterizing samples in fatigue [10] that we repurpose here in the context of LME. The results presented here point to the conclusion that the α' phase formation in unstable austenitic steels is associated with LME sensitivity. We thereby demonstrate here that the LME sensitivity can also be suppressed by tailoring the composition for stability relative to the DIM behavior giving for the first time a sound way out LME concerns in mercury.

Experimental procedures

The composition of the three stainless austenitic steels (304, 316 L and 316L(N)) used in this study is given in Table 1.

The three steels were provided in the annealed metallurgical state. The mean grain size was 40 ± 4 μm for 304 L, 15 ± 2 μm for 316 L and 43 ± 5 μm for 316L(N). The Md_{30} temperature (temperature level at which 50% of the material's volume has undergone martensite transform after 30% plastic deformation) for each of these steels is, respectively of 285 K, 219 K and 129 K according to the Nohara correlation [12].

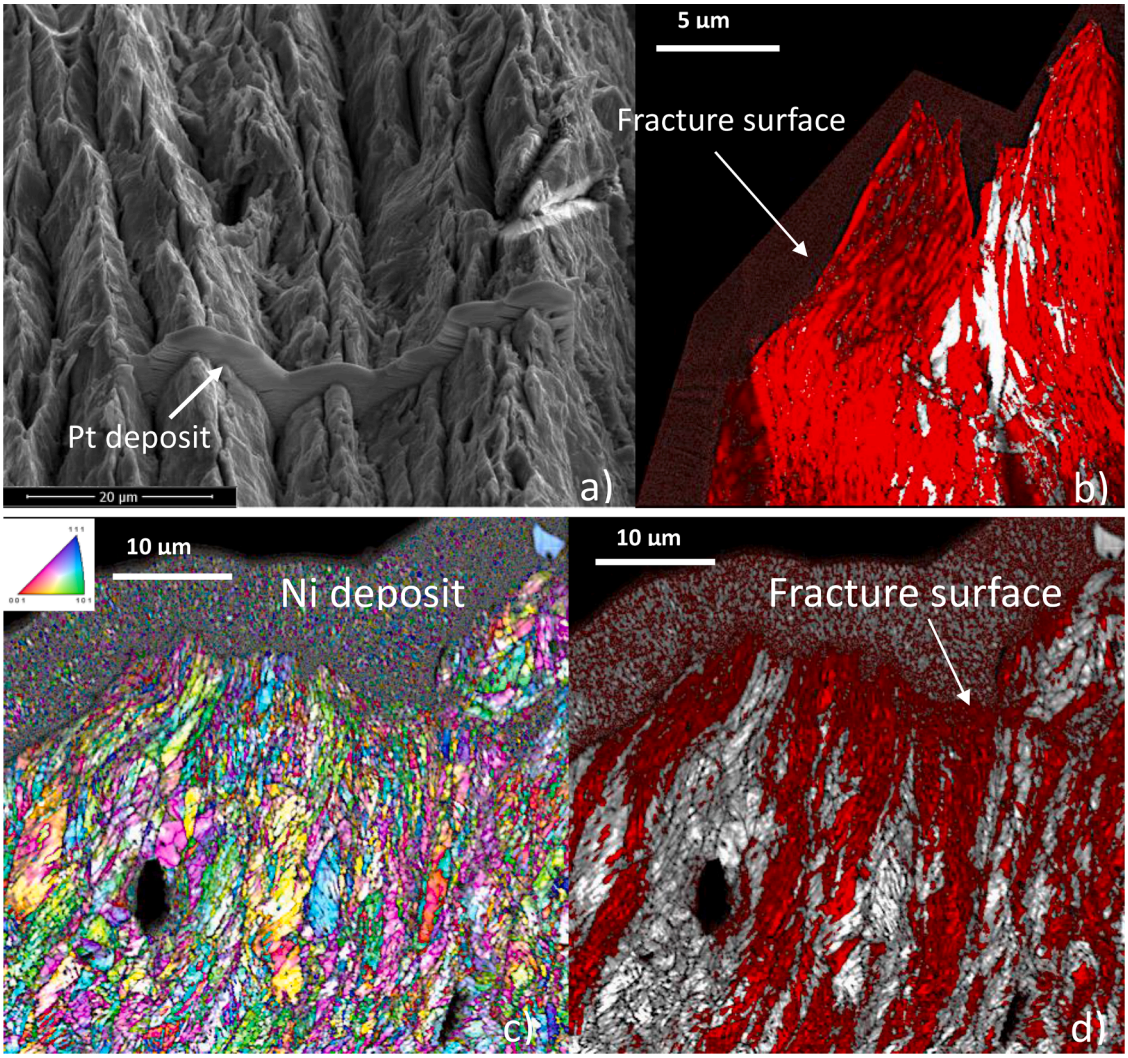

Fig. 1.. 316L-Hg (a) Tilted SEM view of the FIB sampling area with the protective platinum deposit before FIB sectioning (b) t-EBSD phase map of the FIB lamella with Image Quality (IQ) gray coding (α' iron in red) (c) Inverse pole figure (IPF) + IQ map of the coarse-grained cross section d) Corresponding coarse-grained phase map with IQ gray coding relative to c) (α' iron in red). All images are taken from slow strain rate CCT samples at room temperature.

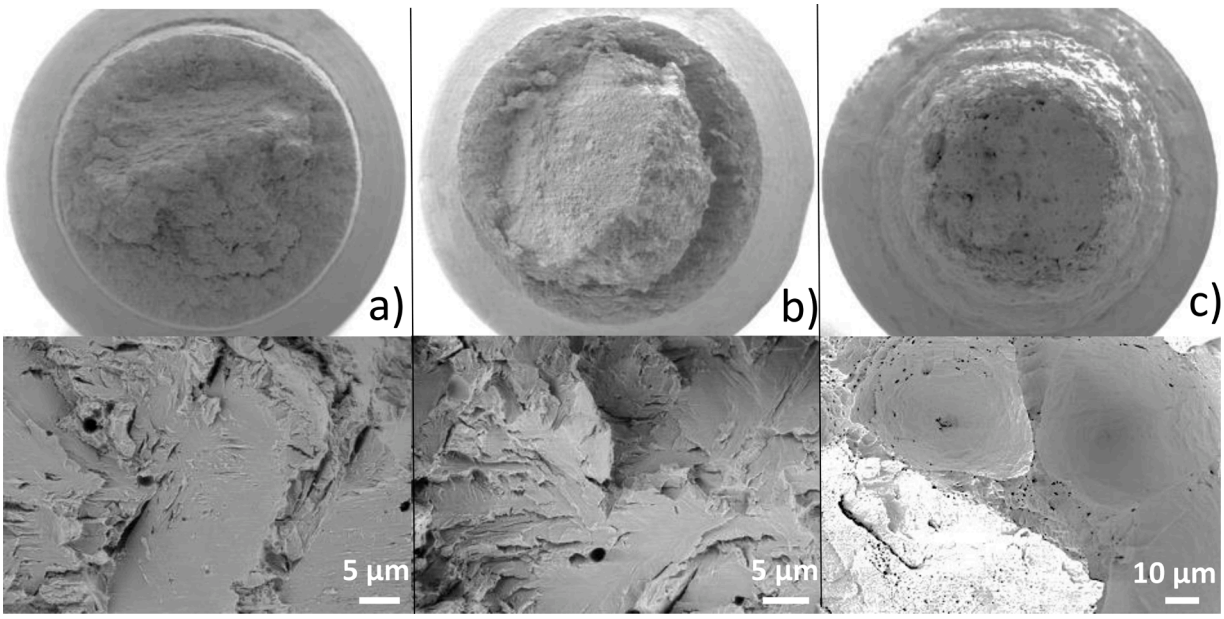

Fig. 2.. Fractographic analysis by SEM of NA fracture. Upper image taken at low magnification. Lower image is a small-scale view of the upper fracture surface - (a) 304L-Hg (b) 316L-Hg (c) 316L(N)-Hg.

A Center Cracked in Tension (CCT) type sample was tested in contact with mercury. The geometry (thickness of 1.5 mm, width of 50 mm with a centered elliptic void of 10 mm length and 2 mm height) allows to study crack propagation in plane stress condition. The CCT samples were wetted at the notch level and were mechanically loaded at a low cross-head speed in the brittle regime (see schematic in Fig. S10 in Supplementary Materials) [13]. A liquid mercury brittle sub-critical crack propagation occurs inducing a reduction of the order of 50% of the energy to fracture [13,14]. The fracture surface induced by the contact with mercury is atypical in this geometry as it leads to a river pattern that has remained unexplained so far [4]. Such a pattern was a strong motive for the small-scale investigation of the fracture crack path reported here. In addition, Notched Axisymmetric (NA) samples were used for the composition variation study (initial diameter of 4 mm, gauge length of 15 mm and a 60° angle notch of 600 µm depth with a tip radius of the order of 100 µm). Two NA samples of each composition were wetted by mercury using the chemical etching technique known from previous studies [4]. An exposure of the notch to diluted hydrochloric acid (5%) was first applied followed by mercury insertion using a variable microliter volume pipette. Mercury readily wets the notch tip ensuring also adherence of the liquid metal drop during mounting manipulations. All mechanical tests were carried out at room temperature in air. The NA wetted samples were tested at two strain rates (1.67×10^{-7} m.s^{-1} and 5.0×10^{-8} m.s^{-1}). Reference NA samples were also tested at 1.67×10^{-7} m.s^{-1}. This notched geometry allows to measure quantitatively the degree of embrittlement when in contact with the liquid metal by a comparative measurement of the energy to fracture. The ratio of that energy by the one for the reference test gives a direct measure of the degree of embrittlement (the mean value of the two wetted measurements is taken here).

After mechanical testing, all the samples were cleaned from mercury by ultrasonic cleaning in distilled water repeated 2 to 3 times to remove mercury. The CCT sample, to be analyzed by EBSD, was electrochemically covered with a nickel deposit of roughly 100 µm. Transverse cuts on the CCT and NA samples were prepared using masked argon ion beam milling (Cross-Polisher from Jeol). EBSD orientation mapping was carried out using a FEG-SEM (FEI Helios 650) in the vicinity of the fracture surface. The gallium focused Ion Beam column of the Helios 650 was used to machine a transmission electron microscope (TEM) lamella at a selected location on a CCT sample (Fig. 1a). The TEM lamella was investigated using EBSD in transmission mode (t-EBSD) at a sample tilt of +38° relative to the EBSD setup. The scanning step could then be reduced down to 10 nm. Two phases (bcc and fcc iron) were allowed in EBSD pattern indexing analysis.

The NA samples were also characterized by X-Ray fractography. The phases in the volume immediately beneath the fracture surface are analyzed using the small X-Ray penetration depth of 40 keV X-Rays in a $\theta-2\theta$ diffraction geometry (it does not exceed a few µm) [10]. The X-Ray diffraction spectra were acquired by focusing the beam onto the fracture surface using a blocking collimator. An amorphous polysiloxane film was inserted covering the notch areas to avoid counting machining induced phase change. A semi-quantitative analysis of the spectra can be conveyed to differentiate the γ (fcc) and α' (bcc) phases. In spite of the unavoidable spread in half-width due to height unevenness, the peaks from the two phases are sufficiently separated to be quantified without ambiguities (here between 44° and 100°). The error estimate of this semi-quantitative analysis is then estimated according to standard procedure at 3% level [15].

Results and discussion

The unusual fracture surface is shown by SEM in Fig. 1a. One can notice the river pattern along which crack propagation proceeds (perpendicularly to the platinum deposit used for the FIB lift-out, indicated by the white arrow). The result of t-EBSD mapping for the 316L-Hg CCT material on the FIB lift-out is shown in Fig. 1b with the phase map (α' iron in red) superposed with the image quality in grey. One can notice that in the probed area, the zone immediately below the fracture surface has almost entirely turned up into α' phase relative to the initial microstructure. The IPF maps (Fig. S1 in Supplementary Materials) demonstrate that fracture proceeds in an interfacial manner in a heavily deformed microstructure. The larger view obtained by conventional EBSD (CCT specimen) reveals that numerous twinning interfaces as well as grain refinement compared with the initial grain size of 15 µm both develops during straining (Fig. 1c, the black spots in the scan are due to ductile cavities growth). The phase map in Fig. 1d shows the banded structure of α' martensite phase transforms in this sample. This is reminiscent of the fluctuations in local chemical composition in the through-thickness direction, an effect of the chemical inhomogeneities resulting from solidification that are not annealed out in fast casting

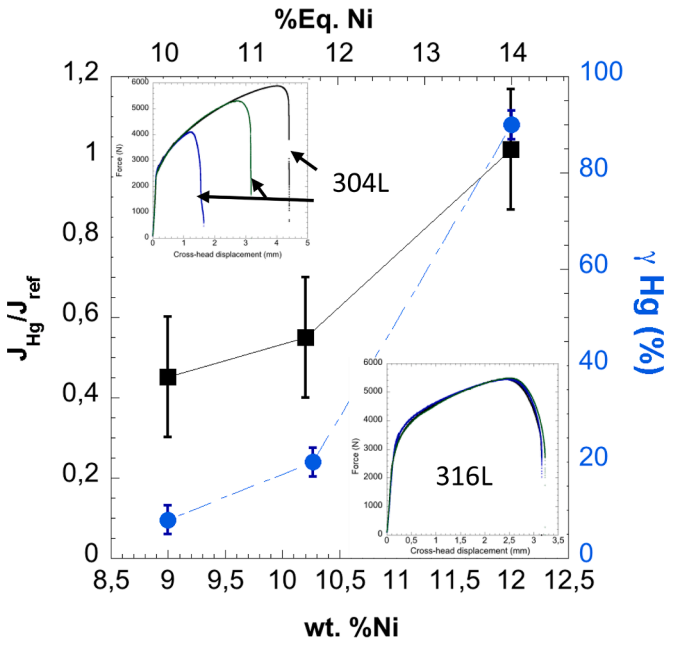

Fig. 3.. Left) Energy to fracture normalized to the reference test (in black). Right) Quantification of the γ phase by X-Ray fractography (in blue). Upper left insert) Force versus Cross-head displacement curves for 304 L austenitic steel (Blue and green in contact with mercury). Lower right insert) Force versus Cross-head displacement curves for 316L(N) austenitic steel.

processes. Local variation in nickel content most likely trigger a higher sensitivity to DIM in low nickel banded areas (Figs. S2–S5 in Supplementary Materials).

The NA samples fractographic analysis is shown in Fig. 2. The mechanical tests results are shown in Fig. 3.

Clearly only the 304 L (9%Ni) and the 316 L (10.2%Ni) show a reduction in energy to fracture (Fig. 3) associated with a change in fracture surface (Fig. 2). At high magnification, one would classify the embrittlement as a "quasi-clivage" fracture mode in the NA geometry. The embrittlement is rated at a factor of two decrease for both steels. This is similar to the ratio found by fracture mechanics experiments for the same 316 L steel (although these tests were carried out in plane stress condition using the CCT geometry) [4]. The onset of embrittlement is seen also after a significant amount of plastic deformation notwithstanding the geometry (CCT or NA). After a sudden crack initiation at macroscopic scale, further crack propagation is sub-critical in the NA geometry as well.

The stunning result of this work is the absence of LME for 316L(N). Neither fractography nor the energy to fracture hints at any LME. The fracture surface looks entirely ductile even at the notch tip location. When considering the X-Ray fractography analysis, one sees a clear difference between the two embrittled steels (304 L and 316 L) and the immune steel (316L(N)). The raw diffractogram for the three steels can be found in supplementary (Fig. S6 in supplementary). The embrittlement is clearly correlated with the amount of DIM probed immediately beneath the fracture surface by X-Rays (Fig. 3, right scale). Overall, these results provide strong evidences that the deformation induced martensitic transformation is the key element in the LME sensitivity.

The EBSD analysis on transverse cuts on the three steels in the NA geometry are shown in Fig. 4 (the corresponding orientation maps can be found in Supplementary Materials, Figs. S7–S9).

The local EBSD analysis for the three steels confirms completely the large difference between the two low nickel austenitic steels and the higher nickel content one (316L(N)). Transformed areas are nearly absent with 316L(N) as indicated by the absence of α' bcc phase detected by EBSD or its low amount revealed by X-Ray fractography. This is in complete accordance with the known behavior of austenitic steels when varying the nickel content [6]. In the phase maps shown here, the γ/α' interfaces were not found to constitute interfaces able to be weakened by mercury while it formally cannot be excluded.

State-of-the-art local samples preparation techniques (Cross-Polisher and FIB lift-out) allowed local EBSD analysis up to the fracture surface enlightening the LME case that was reported in [4]. It is confirmed by the global phase change quantification obtained by X-Ray fractography. The scenario for the LME mechanism with austenitic steels in mercury is therefore the following: the material is plastically deformed until DIM has produced sufficient density of α'/α' interfaces. Beyond some threshold, crack propagation becomes possible in a 3D complex martensite network. In the course of the crack propagation process, mercury does mostly embrittle these interfaces as it can be seen that cracking takes place mostly in transformed area. It is then clear that because no such phase transformation towards a bcc structure is activated with 316L(N), LME is no longer possible to a significant extent.

The findings of this paper are in full agreement with the work of Krupowicz when considering the steel's composition given by the author [2]. No LME is found with mercury on austenitic steels with a nickel content higher than 12% and as such deemed stable austenitic steels (stability is here to be understood relative to the crystallographic ground state that remains in the fcc structure at any plastic strain). This implies that a sufficient amount of nickel in austenitic steels is able to prevent LME sensitivity. This provides the rationale behind the spread in LME sensitivity response in the literature and emphasizes the critical role of DIM with austenitic steel's LME. A similar conclusion was reached with the eutectic gallium-indium-tin liquid melt environment when varying the temperature [9]. When one reaches a temperature high enough to offset the DIM plastic response, LME sensitivity is suppressed. Temperature is not the only variable therefore one can adjust to avoid LME

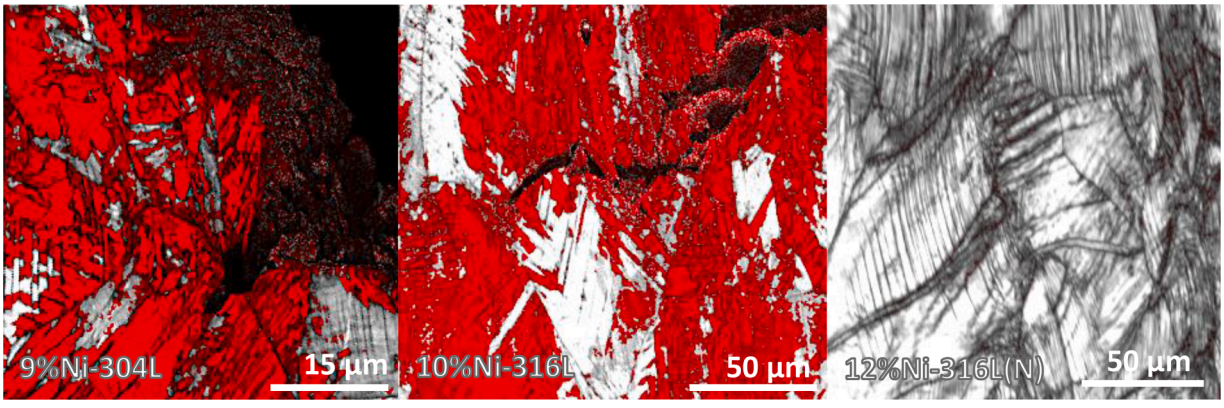

Fig. 4.. EBSD phase maps + IQ on cross-sections for 304 L, 316 L and 316L(N) steels in the NA geometry (α' iron in red).

concern; the steel's composition can also be adjusted to suppress this sensitivity. Whether this procedure is sufficient by itself to maintain an LME insensitivity is to be pondered by the fact that liquid metal corrosion of austenitic steels can lead to nickel depletion by selective leaching in austenitic steel potentially inducing ferritization [16]. This therefore does not preclude to take other measures such as corrosion control in safeguarding against LME.

Conclusion

It has been demonstrated here that a high correlation exists with the occurrence of DIM upon plastic strain in unstable austenitic steels and LME sensitivity at room temperature in mercury. The mechanism of LME requires the formation of α' martensite volume in sufficient amount to manifest itself. The implication for fracture is that principally the bcc crystallographic phase can be embrittled, an empirical finding yet to explain thoroughly. This also raises interesting prospects as to avoid LME concerns in mercury and potentially other liquid metal such as Galinstan or sodium-potassium near room temperature. A careful selection of the material such as a minimum nickel content as in the 316L (N) steel is protective. Structural integrity concerns then shift to ensuring that materials are stable enough in the selected liquid metal environment against ferritization.

Declaration of Competing Interest

The authors declare that they have no known competing financial interests or personal relationships that could have appeared to influence the work reported in this paper.

Acknowledgments

The Helios 660 FIB-SEM work was carried out using the equipment of the MATMECA consortium at CentraleSupélec partially funded by the French ANR under contract number ANR-10-EQPX-37. Sokona Konaté is thanked for her help with the Jeol Cross Polisher. Jean Louis Courouau is thanked for providing the 316L(N) steel. It is a pleasure for one of the authors (T.A.) to acknowledge many pleasant and inspiring discussions on this topic with André Pineau from the Ecole des Mines de Paris (Mines-ParisTech).

Supplementary materials

Supplementary material associated with this article can be found, in the online version, at doi:10.1016/j.scriptamat.2022.114733.

References

[1] X. Gong, M.P. Short, T. Auger, E. Charalampopoulou, K. Lambrinou, Prog. Mater. Sci. 126 (2022), 100920.
[2] ASTM STP 1210 J.J. Krupowicz, R.D. Kane, Slow Strain Rate Testing for the Evaluation of Environmentally Induced Cracking: Research and Engineering Applications, Kane R.D. Philadelphia, 1993, pp. 193–201.
[3] H. Tian, et al., Metall. Mater. Trans. A 37A (2006) 163–173.
[4] L. Medina-Almazan, T. Auger, D. Gorse, J. Nucl. Mater. 376 (2008) 312–316.
[5] J. Talonen, H. Hänninen, Acta Mater. 55 (2007) 6108–6118.
[6] A. Das, S. Tarafder, P.C. Chakraborti, Mater. Sci. Eng. A 529 (2011) 9–20.
[7] B. Barkia, T. Auger, J.L. Courouau, J. Bourgon, Corros. Sci. 127 (2017) 213–221.
[8] B. Barkia, T. Auger, J.L. Courouau, J. Bourgon, J. Mater. Res. 33 (2018) 121–129.
[9] T. Auger, V. Michel, L. Cassayre, H. Baketi, B. Barkia, A. Michel, E. Perrin, Corros. Sci. 192 (2021), 109850, https://doi.org/10.1016/j.corsci.2021.109850.
[10] K. Rajanna, B. Pathiraj, B.H. Kolster, Eng. Fract. Mech. 54 (1996) 155–166.
[11] L. Pryce, K.W. Andrews, J. Iron Steel Inst. 195 (1960) 415–417.
[12] K. Nohara, Y. Ono, N. Ohashi, J. Iron Steel Inst. Jpn. 63 (1977) 212–222.
[13] L. Medina-Almazàn, Etudes Expérimentale Et Numérique De L'effet Du Mercure Sur Le Comportement Mécanique Des Aciers 316 L et T91, Doctoral Dissertation, Ecole Centrale, Chatenay-Malabry, France, 2008.
[14] T. Auger, Z. Hamouche, L. Medina-Almazan, D. Gorse, J. Nucl. Mater. 377 (2008) 253–260.
[15] ASTM E975–13, Standard Practice for X-Ray Determination of Retained austenite in steel with near random crystallographic orientation, in: Proceeding of the ASTM International, West Conshohocken, PA, ASTM, West Conshohocken, PA, 2013. http://www.astm.org.
[16] P. Hosemann, D. Frazer, E. Stergar, K. Lambrinou, Scr. Mater. 118 (2016) 37–40.